ARTICLE

In situ Raman monitoring of electroreductive dehalogenation of aryl halide at Ag/ aqueous solution interface

Received 00th January 20xx,
Accepted 00th January 20xx

DOI: 10.1039/x0xx00000x

Ying-Hua Zhou [a,b,#], Chen-Chen Jiang [b,#], Zhou Yu [b,#], Ya-Hao Wang [b,*], Ju-Fang Zheng [b,*], Xiao-Shun Zhou [b,*]

The electroreductive dehalogenation as an efficient and green approach has attracted much attention in pollution remediation. Herein, we have employed shell-isolated nanoparticle-enhanced Raman spectroscopy (SHINERS) technique to in situ probe the electroreductive dehalogenation process of aryl halides with thiol groups at Ag/aqueous solution interfaces. It is found that the 4-bromothiophenol (BTP) and 4-chlorothiophenol (CTP) can turn into mixture products of 4,4'-biphenyldithiol (BPDT) and thiophenol (TP) as the electrode potential decrease. The conversion ratios estimated by the Raman intensity variations of C-Cl and C-Br vibrations are 44% and 58% for CTP and BTP in the neutral solution, respectively. Furthermore, quantitative analysis of benzene ring vibrations reveals a C-C cross coupling between the benzene free radical interme-diate and adjacent TP product, which results in increased selectivity for biphenyl products at negative potentials.

Introduction

Halogenated organic compounds have been widely applied in the production of cosmetics, medicines, pesticides, flame retardants, etc. Unfortunately, halogenated hydrocarbons are not easy to degrade in the natural environment and can accumulate in the body due to their good physical and chemical stability and acid resistance.[1,2] This results in widespread distribution of halogenated organic pollutants (HOPs), posing a threat to the environment and biological health. Therefore, many technologies have been developed to destroy the strong C-X bonds (X = F, Cl, Br, I), such as biodegradation,[3,4] chemical treatment,[5] ionizing radiatio,[6] photochemistry.[7,8] Recently, the electrochemical strategy that uses electron as a clean reactant provides an efficient and green tool for the reductive dehalogenation of HOPs, has attracted increasing attention over the past decade.[1,2] Meanwhile, continuous efforts have been made to elucidate the electroreductive dehalogenation mechanisms.[9-12] Various techniques, such as cyclic voltammograms,[13] nuclear magnetic resonance[14] and gas chromatography–mass spectrometry[15] have been employed to investigate the electron transfer coefficient and reaction intermediates. However, the aforementioned techniques lack in situ characterization of transient chemical structures at the electrode/liquid interfaces.[16,17] Thus, the interface molecular information for understanding electrocatalytic processes and mechanisms of C–X bond breaking is still rare.

Surface enhanced Raman spectroscopy (SERS)[18-21] is one of the most powerful surface analysis techniques due to its non-destructive, ultra-high sensitivity and freedom from water interference, which has been widely used to probe molecular adsorption and reaction processes,[22-24] including in situ monitoring of C–X bond dissociation.[11] However, it is found that the plasmon-generated hot electrons on Au and Ag nano-particles can activate the C–X bond of halogenated organic compounds and enable the C-C cross coupling process.[25-27] This indicates that conventional SERS cannot be directly used to study the electrochemical dehalogenation process due to surface plasmon interference. A recently developed novel Raman technique called shell-isolated nanoparticle-enhanced Raman spectroscopy (SHINERS)[28-31] can overcome the above-mentioned problems of traditional SERS, which uses a plasmon-activated Au or Ag cores coated with ultra-thin silica shells as the Raman signal amplifiers. Because the chemically inert silica shell prevents hot electrons on the plasmonic metal core from contaminating the reaction process.[32-34] Therefore, SHINERS provides a good platform for studying the electrochemical reductive dehalogenation process.

In this work, the SHINERS was used to in situ monitor the electroreductive dehalogenation process of 4-bromothiophenol (BTP) and 4-chlorothiophenol (CTP) at Ag/ aqueous solution interface. The effects of applied potential and pH of the aqueous solution on the cleavage of C-X bond were systematically investigated. As decreasing the potentials of electrodes, the Raman spectroscopic features demonstrated the mixture products of 4,4'-biphenyldithiol (BPDT) and

[a] Jinhua Education College, Jinhua 321000, China
[b] Key Laboratory of the Ministry of Education for Advanced Catalysis Materials, Institute of Physical Chemistry, Zhejiang Normal University, Jinhua 321004.
E-mail: jfzheng@zjnu.cn; yahaowang@zjnu.edu.cn; xszhou@zjnu.edu.cn
# These authors contributed equally.

thiophenol (TP). Furthermore, the product selectivity and reaction mechanism were analysed by the potential-dependent intensity variations of the Raman bands. The present work provides molecular-level insights into the electrochemical reduction of carbon-halogen (C-X) bonds in aqueous solutions.

Experimental

Reagents and materials

4-Chlorothiophenol (98%) and 4-bromothiophenol (97%) were purchased from Alad-din Biochemical Technology Co., Ltd. 4,4'-Biphenyldithiol (97%) was purchased from Jilin Chinese Academy of Sciences-Yanshen Technology Co., Ltd. and sodiumthiophenoxide (97%) was purchased from Beijing Inno-Chem Technology Co., Ltd. The $NaClO_4$ (99%), $HClO_4$ (50%) and NaOH (95%) were purchased from Alfa-Asia Chemical Co., Ltd. All chemicals were used as received, and all aqueous solutions were prepared with ultrapure water (>18.2 M Ω cm).

Electrochemical measurements

The cyclic voltammograms (CVs) were performed at a CHI-660E potentionstat using a homemade three-compartment glass cell. The saturated calomel electrode (SCE) and Pt were used as reference and counter electrodes, respectively. A smooth electrode Ag electrode was used as the work electrode. The solutions in electrochemical measurements were deaerated and protected by argon.

Preparation and characterization of nanoparticles

According to previous reports,[35] the 55 nm Au nanospheres were synthesized ac-cording to the following procedure: 1.4 mL of sodium citrate solution (1 wt%) was quickly added into 200 mL of boiling $HAuCl_4$ solution (0.01 wt%). Then the mixture was refluxed for 20 min to obtain the spherical nanoparticles with a diameter ca. 55 nm. Finally, the Au colloidal solution was cooled to room temperature in ambient atmosphere for the prepa-ration of Au @ SiO_2 nanoparticles.

The 55 nm Au @ ca. 2 nm SiO_2 nanoparticles were prepared according to following procedures: 0.4 mL of (3-Aminopropyl) trimethoxysilane solution (1 mM) was dropwise added into 30 mL of the as-prepared Au solution under stirring at room temperature. Next, 3.2 mL of sodium silicate solution (0.54 wt%) was quickly added to the solution, then transferred to 99°C water bath and stirred for 30 min. Finally, pipette 1.5 mL of the hot solution into a centrifuge tube and immediately immerse it in ice bath to stop the reaction. The solution was centrifuged at 4500 rpm and washed twice with Milli-Q water for the Raman measurements.

Electrochemical Raman measurement

The Raman measurements were carried out on a confocal microscope Raman system (Renishaw InVia). A He-Ne laser with 632.8 nm excitation wavelength and a 50× micro-scope objective with a numerical aperture of 0.55 was used in all Raman measurements. In situ electrochemical Raman experiment was carried out in homemade Raman cell with potential control by CHI-660D potentiostat at a quasi-steady-state condition, when the current rapidly decrease to a to a low value after applying the specific potential in few minutes. Each Raman spectrum was acquired over a collection time of 10 s, the laser intensity is 163 μW/ cm^2.

Results and discussion

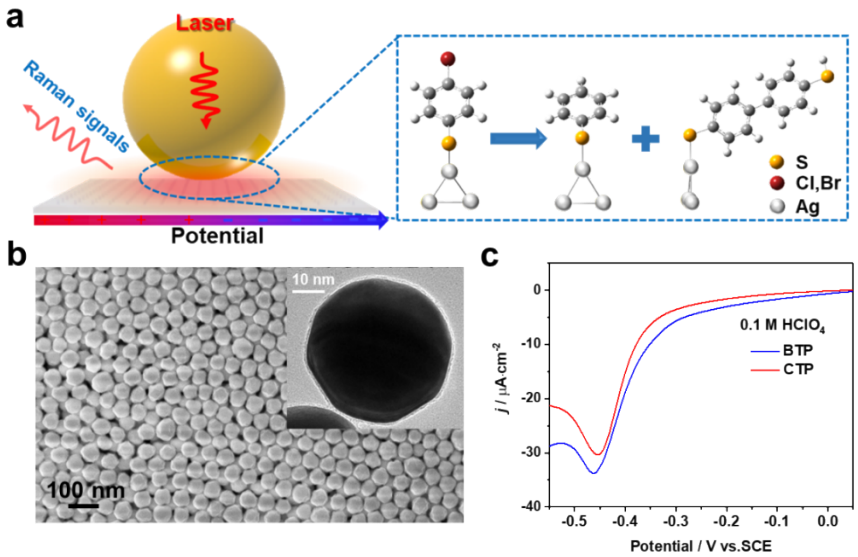

Fig. 1 (a) Schematic diagram of electrochemical SHINERS for probing electroreductive dehalogenation of aryl halides at Ag surface. (b) SEM and TEM images of as-prepared Au@ SiO_2 nanoparticles for Raman measurements. (c) CVs of CTP and BTP adsorbed on smooth Ag electrode in 0.1 M $HClO_4$ (pH=1) with a scan rate 0.1 V/s.

ARTICLE

In situ Raman for probing electroreductive dehalogenation processn

Fig. 1a schematically illustrates the SHINERS technique used to probe the electroreductive dehalogenation process of aryl halides with thiol bonds absorbed on the smooth Ag electrode. The BTP or CTP molecules are assembled on the electrode surface through the thiol groups in an ethanol solution containing 1 mM target molecules. Then the as-prepared 55 nm Au @ ca. 2 nm SiO_2 nanoparticles (Fig. 1b) are dropped on the surface as Raman signal amplifiers, which can generate up to 10^8 times stronger electromagnetic fields to enhance Raman vibrational signals under laser irradiation.[36] The ultra-thin and inert silica shells can prevent generating interference Raman signal from the Au core as well as the SPR induced C–X bond cleavage.[10]

Fig. 1c shows the cyclic voltammograms (CVs) of CTP and BTP assembled on smooth Ag electrode recorded in 0.1 M $HClO_4$ with a scan rate of 0.1 V/s. There are cathodic peaks located at about -0.45 V, corresponding to the reductive desorption of the thiolate molecules from the Ag surface consistent with previous reports.[10,37] Therefore, the dehalogenation reduction current is buried in the cathodic current for molecular desorption. Voltametric data alone cannot help reveal the exact origin of electrochemical dehalogenation in aqueous solutions.

Then, we employed SHINERS to in situ probe the electrochemical process of CTP and BTP assembled on smooth Ag electrode in 0.1 M $HClO_4$ as changing the potentials from 0.4 V to -0.4 V vs. SCE. Fig. 2a shows the potential-dependent spectra with 0.1 V intervals. At the initial potential of 0.4 V, the characteristic Raman peaks of CTP molecules can be observed. Consistent with previous reports,[10] the intense peaks at 1065, 1085 and 1570 cm^{-1} are attributed to a hybrid mode of phenyl ring and C–Cl vibrations, C–S stretching mode (ν(C–S)) and the symmetric stretching mode of benzene ring (ν(CC)), respectively.

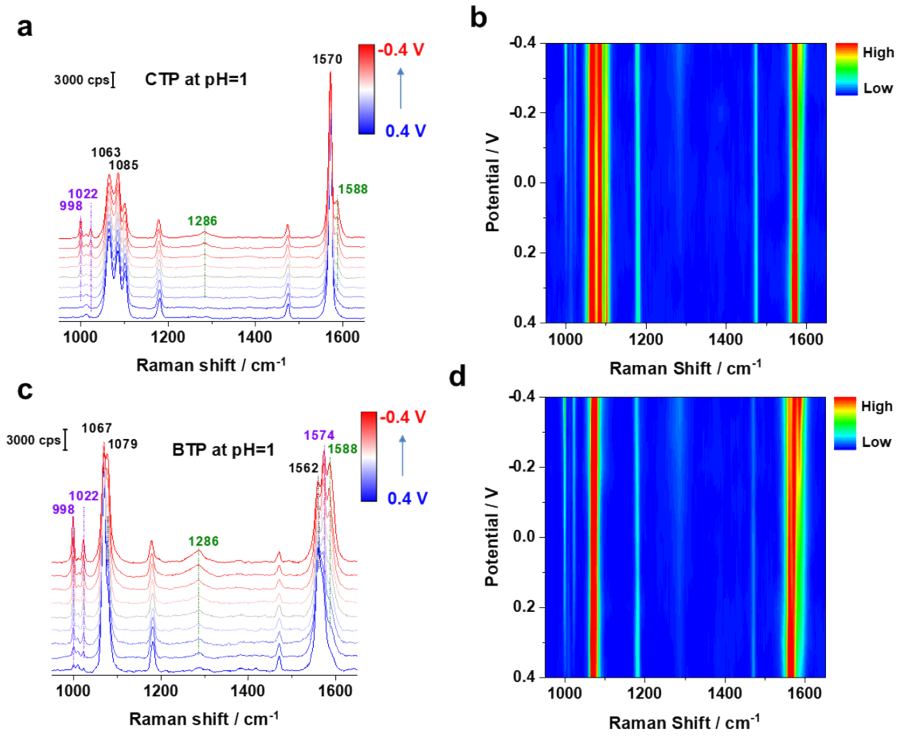

Fig. 2 Potential-dependent Raman spectra of (a) CTP and (c) BTP on Ag electrode in 0.1 M $HClO_4$ solution (pH=1) at different potentials. The color-coded intensity map of potential-dependent spectra of (d) CTP and (d) BTP on Ag electrode in 0.1 M $HClO_4$ solution (pH=1).

As the potential decreases, Raman bands at 998,1022, 1286 and 1588 cm^{-1} appear and become stronger, in contrast to the decreased intensity of Raman band at 1065 cm^{-1}. These can further be confirmed in the color-coded intensity map of potential-dependent spectra in Fig. 2b. According to previous reports,[26,38] these Raman bands at 998 and 1022 cm^{-1} are assigned to a hybrid mode of CC stretching + benzene ring in-plane deformation and C-H deformation of TP. These Raman bands at 1286 and 1588 cm^{-1} are ascribed to the stretching between two phenyl rings and symmetric stretching mode of the phenyl ring of BPDT. Similarly, the potential-dependent Raman spectra of BTP on Ag surface also present characteristic Raman peaks of TP and BPDT in Fig. 2c and d. In addition, the ν(CC) of BTP at 1562 cm^{-1} can be distinguished from TP and BPDT. The SHINERS spectra of commercial TP and BPDT adsorbed on smooth Ag electrode in Fig. S1 further confirm the reduction products of CTP and BTP. These clearly demonstrate the CTP and BTP on Ag electrode can undertake electrochemical reduction and turn into TP and BPDT products as potential negatively scan. In addition, the biphenyl product indicates that the cleavage of the C-X bond involves a C-C coupling process.

The pH effects

It is reported that the electroreductive dehalogenation mechanism involves direct electron transfer and electrocatalytic hydrodehalogenation on the electrode surface.[2,9,39] Typically, the latter one need active atomic hydrogen for C-X bond cleavage.[40] Thus, the polarity and pH of solution might have an impact on the electrochemical reduction of CTP and BTP on smooth Ag electrode. To examine the pH effect, we further used in situ electrochemical SHINERS to probe the electrochemical processes of CTP and BTP on smooth Ag electrode in 0.1 M $NaClO_4$ (pH=7). The potential-dependent Raman spectra in Fig. 3a and c clearly show that the new Raman bands assigned to the products of TP and BPDT appears as potential decreases.

Quantitatively, the Raman band intensity variation of ν(C−Cl) and ν(C−Br) are used to estimate the catalytic conversion rate of dehalogenation, using $(I_0\text{-}I)/I_0$, where I_0 and I the initial band intensities at 0.4 V and a specific potential, respectively. As shown in Fig. 3b and d, the potentials for observing the

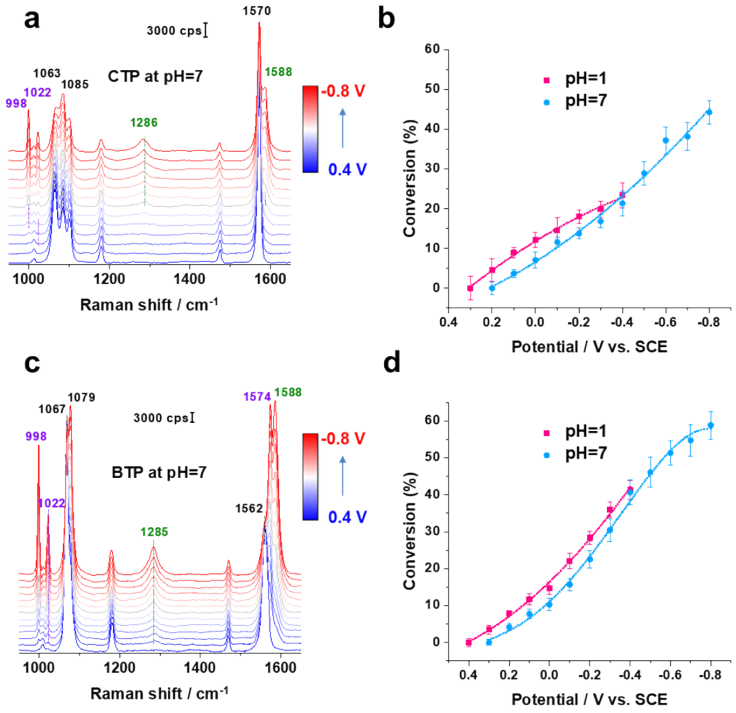

Fig. 3 The potential-dependent Raman spectra of CTP (a) and BTP (c) on Ag electrode in 0.1 M $NaClO_4$ solution (pH=7). The conversion ratios of C−Cl (b) and C-Br (d) cleavages against the applied potentials at pH=1 (red line) and 7 (blue line).

cleavage of C–Cl and C-Br bonds at pH=7 both are 0.1 V more negative than that at pH=1. Interestingly, the potential-dependent conversion ratios of CTP and BTP at pH =1 both are larger than that at pH=7 at the same electrode potentials vs. SCE. These suggest that the electrochemical reduction of aryl halides on the Ag electrode can proceed via a hydrochlorination mechanism. The higher activity in acid solution arises from much more protons in the acid solution to facilitate the proton transfer and formation of active atomic hydrogen for C-X bond cleavage.

In addition, the conversion ratios of C–X bond rapidly growth as the electrode potentials decrease. Finally, a 41 % conversion is achieved for BTP at -0.4 V compared to 23 % for CTP at pH=1, which are limited by the heavy hydrogen evolution and molecular desorption. Similarly, a larger conversion rate of 58% (BTP) can be observed 44% (CTP) and at -0.8 V in neutral solution. This is due to the higher bond dissociation energies for the cleavage of C–Cl bond compared to that of C-Br bond. Typically, changing the pH of solution from 1 to 7, the equilibrium potential for hydrogen evolution should be with a calibration of -0.35 V respect to reversible hydrogen electrode (RHE). While the potentials for observing the cleavage of C–X bonds only change 0.1 V. This incomplete pH-dependent behaviour further suggests that electrochemical reduction via a direct electron transfer mechanism may also be involved. Thus, direct molecular evidences obtained by SHINERS demonstrate electroreductive dehalogenation of CTP and BTP can via electrocatalytic hydrodechlorination and direct electron transfer in acidic and neutral aqueous solutions.

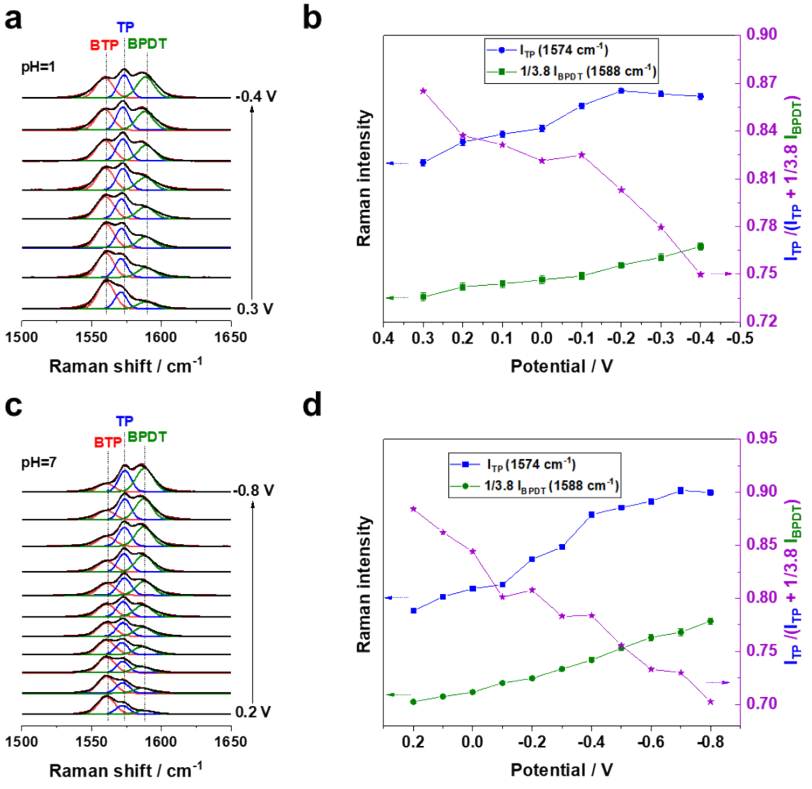

Fig. 4 Electrochemical potential-dependent spectra of benzene ring CC stretching vibration (ν(CC)) with Gaussian peak fitting during BTP reduction at pH=1 (a) and 7 (c). The plot of ν(CC) intensity variation of I_{TP} (blue squares) and 1/3.8 I_{BPDT} (green square) against the potentials of electrode in at pH=1 (b) and 7 (d). The purple stars represent product selectivity of TP on the surface derived from $I_{TP}/(I_{TP}$ +1/3.8 $I_{BPDT})$.

Electroreductive dehalogenation mechanism

For insight into the electroreductive dehalogenation process, we further use the CC stretching vibration of the benzene ring (ν(CC)) in TP and BPDT to quantify the reduction products of BTP. As the ν(CC) wavenumbers are almost the same in CTP and TP (Fig. 1a and 2a), we cannot perform the same analysis for CTP. Fig. 4a and c show the potential-dependent spectra for the specific range 1500-1650 cm^{-1} at 0.1 V intervals. The three distinct bands at 1562, 1574 and 1588 cm^{-1} are ascribed to the ν(CC) of BTP, TP and BDTP, respectively. Typically, Raman band intensities are directly proportional to the surface coverage of analytes in the same SERS "hotspot". Therefore, we use the same ν(CC) mode intensity for TP and BPDT to analysis the relative amount of surface species.

To represent the relative amount of surface species, it should be noted that the peak areas of ν(CC) were corrected by a ratio of 1:3.8 (TP: BPDT) according to the different SERS cross-sections of the surface species in the reported SERS measurements.[10,41] With Gaussian peaks fitting, the ν(CC) intensity of TP (I_{TP}, blue squares) and BPDT (I_{BPDT}, green circles) are plotted against the potentials of electrode in Fig. 4b and d. It can be found that I_{TP} is much larger than 1/3.8 I_{BPDT} at pH = 1 and 7, which indicates that TP is the main product of the electrochemical reduction at the studied potentials

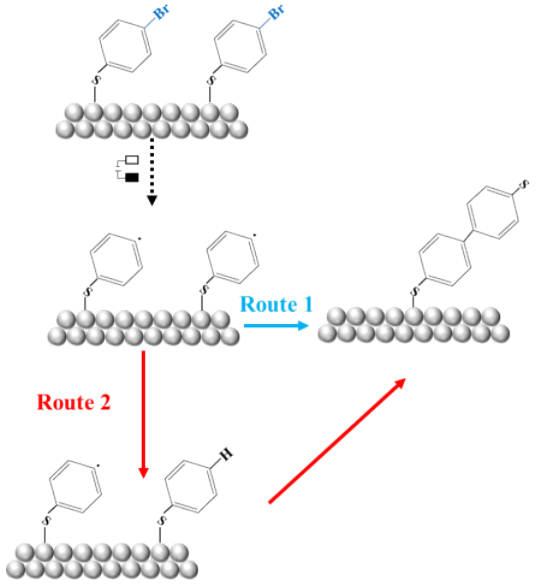

Fig. 5 Proposed reaction pathways for electroreductive dehalogenation of BTP towards BPDT on Ag surface.

Next, the product selectivity of TP on the surface is estimated by using I_{TP} / (I_{TP} +1/3.8 I_{BPDT}). As shown in Fig. 4b and d (purple stars), TP selectivity was found to be as high as about 90% at an initial positive potential and then fluctuated down to 75% at pH = 1 and 68% at pH = 7 with potential decreasing. This may be due to the C-C coupling process required to generate BPDT.

Generally, there are two possible reaction pathways for C–C bond formation during the electrochemical reduction of BTP. As shown in Fig. 5, firstly, BTP is reduced via direct electron transport or active atomic hydrogen to form benzene radical (Ar·), which is a widely reported key intermediate in electroreductive dehalogenation.[9,42] Then, two adjacent Ar· can undergo an Ullmann-type self-coupling reaction to form a BPDT (Route 1). Second, Ar· can be further reduced by the cathode and combined with H^+ in solution to generate TP product. Then TP product and another Ar· undergo a cross-coupling reaction to form BPDT (Route 2).

In Fig. 4b and d, it can be found that the product selectivity of TP decreases with decreasing potential. This indicates that much more Ar· is generated at negative potentials, which increases the possibility of Ullmann-type self-coupling of two adjacent Ar· to form BPDT. On the other hand, I_{TP} decreases below −0.2 V at pH = 1 and below −0.7 V at pH = 7, compared to the steady rise of I_{BPDT}. This indicates the TP product reacts with the Ar· and turns into BPDT at these negative potentials. This further reveals the mechanism of electroreductive dehalogenation of BTP including a cross-coupling reaction between Ar· and TP product.

Conclusions

To conclusion, the electroreductive dehalogenation process of CTP and BTP at Ag /aqueous solution interfaces have been successfully investigated with in situ SHINERS method. The mixture reduction products of TP and BPDT have been confirmed in acidic and neutral solutions. As the electrode potentials decrease, the conversion estimated by the Raman intensity variations of C-Cl and C-Br vibrations show a higher catalytic activity in acidic solution. But the applied potential is limited by the hydrogen evolution reaction and molecular desorption, resulting in 44% and 58% conversions of CTP and BTP at pH = 7, respectively. This quantitative analysis of C-X bond and benzene ring vibrations of products suggests the electroreductive dehalogenation of CTP and BTP via reduction both by atomic hydrogen and direct electron transfer. At the negative potentials, the benzene free radical intermediate can react with adjacent TP product to increase selectivity for biphenyl products. This present work provides a molecular-level insight into the electroreductive dehalogenation at Ag electrode.

Conflicts of interest

There are no conflicts to declare.

Acknowledgements

We are thankful for financial support from the National Natural Science Foundation of China (Nos. 22102150, 22172146 and 21872126), the Zhejiang Provincial Natural Science Foundation of China (No. LQ21B030010) and the Science and Technology Project of Jinhua (2021-4-378).

Notes and references

1. Q. Zhuo, J. Lu, J. Niu, J. C. Crittenden, G. Yu, S. Wang, B. Yang and Z. Chen, ACS ES&T Engg., 2022, **2**, 1756-1775.
2. E. T. Martin, C. M. McGuire, M. S. Mubarak and D. G. Peters, Chem. Rev., 2016, **116**, 15198-15234.
3. P. Bhatt, M. S. Kumar, S. Mudliar and T. Chakrabarti, Crit. Rev. Environ. Sci. Technol.,2007, **37** , 165-198.
4. B. G. Kwon, H.-J. Lim, S.-H. Na, B.-I. Choi, D.-S. Shin and S.-Y. Chung, Chemosphere, 2014, **109**, 221-225.
5. C. D. Vecitis, H. Park, J. Cheng, B. T. Mader and M. R. Hoffmann, J. Phys. Chem. C., 2008, **112**, 16850-16857.
6. M. Trojanowicz, I. Bartosiewicz, A. Bojanowska-Czajka, K. Kulisa, T. Szreder, K. Bobrowski, H. Nichipor, J. F. Garcia-Reyes, G. Nałęcz-Jawecki, S. Męczyńska-Wielgosz and J. Kisała, Chem. Eng. J., 2019, **357**, 698-714.
7. U. Rao, Y. Su, C. M. Khor, B. Jung, S. Ma, D. M. Cwiertny, B. M. Wong and D. Jassby, Environ. Sci. Technol., 2020, **54**, 10668-10677.
8. Y. Su, U. Rao, C. M. Khor, M. G. Jensen, L. M. Teesch, B. M. Wong, D. M. Cwiertny and D. Jassby, ACS Appl. Mater. Interfaces., 2019, **11**, 33913-33922.
9. H. Yin, X. Cao, C. Lei, W. Chen and B. Huang, ChemElectroChem., 2020, **7**, 1825-1837.
10. C.-C. Jiang, X.-C. Li, J.-A. Fan, J.-Y. Fu, X.-N. Huang-Fu, J.-J. Li, J.-F. Zheng, X.-S. Zhou and Y.-H. Wang, Analyst, 2022, **147**, 1341-1347.
11. A. Wang, Y.-F. Huang, U. K. Sur, D.-Y. Wu, B. Ren, S. Rondinini, C. Amatore and Z.-Q. Tian, J. Am. Chem. Soc., 2010, **132**, 9534-9536.
12. Y.-F. Huang, D.-Y. Wu, A. Wang, B. Ren, S. Rondinini, Z.-Q. Tian and C. Amatore, J. Am. Chem. Soc., 2010, **132**, 17199-17210.
13. G. Jiang, M. Lan, Z. Zhang, X. Lv, Z. Lou, X. Xu, F. Dong and S. Zhang, Environ. Sci. Technol., 2017, **51**, 7599-7605.
14. U. Bussy, P. Giraudeau, V. Silvestre, T. Jaunet-Lahary, V. Ferchaud-Roucher, M. Krempf, S. Akoka, I. Tea and M. Boujtita, Anal. Bioanal. Chem., 2013, **405**, 5817-5824.
15. K. Zhao, X. Quan, Y. Su, X. Qin, S. Chen and H. Yu, Environ. Sci. Technol., 2021, **55**, 14194-14203.
16. S.-L. Lv, C. Zeng, Z. Yu, J.-F. Zheng, Y.-H. Wang, Y. Shao and X.-S. Zhou, Biosensors, 2022, **12**, 565.
17. C.-P. Tao, C.-C. Jiang, Y.-H. Wang, J.-F. Zheng, Y. Shao and X.-S. Zhou, J. Phys. Chem. Lett., 2020, **11**, 10023-10028.
18. J.-F. Li, Y.-J. Zhang, S.-Y. Ding, R. Panneerselvam and Z.-Q. Tian, Chem. Rev., 2017, **117**, 5002-5069.
19. R. Pilot, R. Signorini, C. Durante, L. Orian, M. Bhamidipati and L. Fabris, Biosensors, 2019, **9**, 57.
20. S. E. J. Bell, G. Charron, E. Cortés, J. Kneipp, M. L. de la Chapelle, J. Langer, M. Procházka, V. Tran and S. Schlücker, Angew. Chem. Int. Ed., 2020, **59**, 5454-5462.
21. J. Zhao, C. Zhang, Y. Lu, Q. Wu, Y. Yuan, M. Xu and J. Yao, J. Raman Spectrosc., 2020, **51**, 2199-2207.
22. H. Zhang, S. Duan, P. M. Radjenovic, Z.-Q. Tian and J.-F. Li, Acc. Chem. Res., 2020, **53**, 729-739.
23. Z. Yu, J.-Q. Li, Y.-H. Wang, J.-Q. Su, J.-Y. Fu, J.-W. Zou, J.-F. Zheng, Y. Shao and X.-S. Zhou, Anal. Chem., 2022, **94**, 1823-1830.
24. J.-Y. Fu, X.-C. Li, Z. Yu, X.-N. Huang-Fu, J.-A. Fan, Z.-Q. Zhang, S. Huang, J.-F. Zheng, Y.-H. Wang and X.-S. Zhou, Langmuir, 2022, **38**, 6209-6216.
25. Y. Zhao, L. Du, H. Li, W. Xie and J. Chen, J. Phys. Chem. Lett., 2019, **10**, 1286-1291.
26. P. Jiang, Y. Dong, L. Yang, Y. Zhao and W. Xie, J. Phys. Chem. C., 2019, **123**, 16741-16746.
27. J. Liu, Z.-Y. Cai, W.-X. Sun, J.-Z. Wang, X.-R. Shen, C. Zhan, R. Devasenathipathy, J.-Z. Zhou, D.-Y. Wu, B.-W. Mao and Z.-Q. Tian, J. Am. Chem. Soc., 2020, **142**, 17489-17498.
28. J.-F. Li, Y.-F. Huang, Y. Ding, Z. L. Yang, S.-B. Li, X.-S. Zhou, F.-R. Fan, W. Zhang, Z.-Y. Zhou, D.-Y. Wu, B. Ren, Z.-L. Wang and Z.-Q. Tian, Nature, 2010, **464**, 392-395.
29. Y.-H. Wang, J.-B. Le, W.-Q. Li, J. Wei, P. M. Radjenovic, H. Zhang, X.-S. Zhou, J. Cheng, Z.-Q. Tian and J.-F. Li, Angew. Chem. Int. Ed., 2019, **58**, 16062-16066.
30. T. A. Galloway and L. J. Hardwick, J. Phys. Chem. Lett., 2016, **7**, 2119-2124.
31. Y.-F. Huang, P. J. Kooyman and M. T. M. Koper, Nat. Commun., 2016, **7**, 12440.
32. S. Guan, O. Donovan-Sheppard, C. Reece, D. J. Willock, A. J. Wain and G. A. Attard, ACS Catal., 2016, **6**, 1822-1832.
33. Z. Yu, Y.-X. Xu, J.-Q. Su, P. M. Radjenovic, Y.-H. Wang, J.-F. Zheng, B. Teng, Y. Shao, X.-S. Zhou and J.-F. Li, Angew. Chem. Int. Ed., 2021, **60**, 15452-15458.
34. Y.-H. Wang, S. Zheng, W.-M. Yang, R.-Y. Zhou, Q.-F. He, P. Radjenovic, J.-C. Dong, S. Li, J. Zheng, Z.-L. Yang, G. Attard, F. Pan, Z.-Q. Tian and J.-F. Li, Nature, 2021, **600**, 81-85.
35. J.-F. Li, X.-D. Tian, S.-B. Li, J. R. Anema, Z.-L. Yang, Y. Ding, Y.-F. Wu, Y.-M. Zeng, Q.-Z. Chen, B. Ren, Z.-L. Wang and Z.-Q. Tian, Nat. Protoc., 2013, **8**, 52-65.
36. Y.-H. Wang, M.-M. Liang, Y.-J. Zhang, S. Chen, P. Radjenovic, H. Zhang, Z.-L. Yang, X.-S. Zhou, Z.-Q. Tian and J.-F. Li, Angew. Chem. Int. Ed., 2018, **57**, 11257-11261.
37. C. Vericat, M. E. Vela, G. Benitez, P. Carro and R. C. Salvarezza, Chem. Soc. Rev., 2010, **39**, 1805-1834.
38. S.-C. Huang, X. Wang, Q.-Q. Zhao, J.-F. Zhu, C.-W. Li, Y.-H. He, S. Hu, M. M. Sartin, S. Yan and B. Ren, Nat. Commun., 2020, **11**, 4211.

39. Y.-Y. Lou, J.-M. Fontmorin, A. Amrane, F. Fourcade and F. Geneste, Electrochim. Acta., 2021, **377**, 138039.
40. R. Mao, C. Huang, X. Zhao, M. Ma and J. Qu, Appl. Catal. B., 2019, **241**, 120-129.
41. Y. Li, Y. Hu, F. Shi, H. Li, W. Xie and J. Chen, Angew. Chem. Int. Ed., 2019, **58**, 9049-9053.
42. A. A. Isse, A. De Giusti, A. Gennaro, L. Falciola and P. R. Mussini, Electrochim. Acta., 2006, **51**, 4956-4964.